Multimolecular-Micelle Formation of Poly(methyl methacrylate)-*graft*-polystyrene in Acetonitrile/(Acetoacetic Acid Ethyl Ether)

Atsushi Kikuchi and Takuhei Nose*

Department of Polymer Chemistry, Tokyo Institute of Technology, Ookayama, Meguro-ku, Tokyo 152, Japan

Received July 26, 1996; Revised Manuscript Received December 6, 1996[⊗]

ABSTRACT: Multimolecular-micelle formation is investigated by means of light scattering for poly(methyl methacrylate)-*graft*-polystyrene with low grafted-chain density in a dilute solution of mixed selective solvent of acetonitrile and acetoacetic acid ethyl ether. Molecular weights of the poly(methyl methacrylate) (PMMA) backbone and the polystyrene (PS) branch are about 5.6×10^6 and 9.2×10^3, respectively, and the grafted-chain density is 13 wt % PS. The mixed solvent is a marginally-good solvent to PMMA and is a nonsolvent to PS. Time evolutions of apparent molecular weight M_{app}, radius of gyration R_{gapp}, and hydrodynamic radius R_{happ} are measured in the course of micellization after quenching from the unimer region to the micelle region. Observed M_{app} dependences of R_{gapp}, R_{happ}, and R_{gapp}/R_{happ} demonstrate the following features of multimolecular-micelle formation. Unimolecular micelles, which are made of a few linearly-connected flowers with small cores of associated PS branches and petals of PMMA backbone, are associated with each other by primarily connecting at the ends of respective end-flowers to form multimolecular micelles of the flower-connecting type. An analysis with a worm-like chain model reveals that the multimolecular micelle is fairly rigid, having the contour length of more than several hundreds of nanometers.

Introduction

Micelle formation of polymer chains in a solution of a selective solvent has extensively been studied from theoretical and experimental points of view.[1−8] Diblock and triblock copolymers form rather simple associated micelles similar to low-molecular-weight surfactants in aqueous solution. On the contrary, multiblock copolymers including graft copolymers may form a variety of micellar structures depending upon the sequence and length of the block chains and the solvent quality by either intra- or intermolecular association. For its importance, a limited number of studies on unimolecular micelles[9−15] and the association structure[9,10,12,13] of multiblock copolymers and graft copolymers have been reported.

In this series of studies, we are concerned with unimolecular micelles and their intermolecular associates formed from graft copolymers with short branch chains of low grafted-chain densities. In previous papers,[16,17] we studied the unimolecular-micelle formation of poly(methyl methacrylate)-*graft*-polystyrene (PMMA-*g*-PS) in solvents selective to the PMMA backbone or PS branches. Estimated structures of the unimolecular micelles are shown in Figure 1. In a solvent selective to the branches, rod-like unimolecular micelles are strongly suggested to be formed by intramolecular segregation between the PMMA backbone and PS branches.[16] On the other hand, in solvents selective to the backbone, rigid-rod-like unimolecular micelles made of a few linearly-connected flowers are formed.[17] In this study, we focus our attention on the multimolecular micelle, i.e., intermolecular associations of these unimolecular micelles.

Here we deal with the association of the unimolecular micelles of type b in Figure 1. Namely, we study the association behavior of graft copolymer PMMA-*g*-PS in a mixed solvent of acetonitrile/(acetoacetic acid ethyl ether), which is the same system as used in the previous study.[17] Static and dynamic light scattering measurements were carried out for the copolymer solutions in the course of micellization after quenching from the unimer region to the micelle region to reveal the formation and the structure of multimolecular micelles.

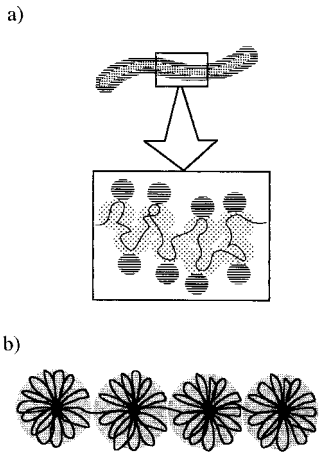

Figure 1. Estimated structure of unimolecular micelle of PMMA-*g*-PS formed in solvent selective to branches (a) or backbone (b).[16,17] In solvent selective to branches, rod-like unimolecular micelles are strongly suggested to be formed by intramolecular segregation between the PMMA backbone and PS branches, with the shrunken PMMA backbone forming the rod-like core covered with PS chains. On the other hand, in solvent selective to the backbone are formed rigid-rod-like unimolecular micelles made of a few linearly-connected flowers with small cores of associated PS branches and petals of PMMA backbone.

Experimental Section

Materials. Poly(methyl methacrylate)-*graft*-polystyrene (PMMA-*g*-PS) was synthesized by the coupling reaction between fractionated PMMA and living PS. In Table 1 are listed characteristics of the graft copolymer. Details of preparation and characterization of the copolymer were described in previous papers.[16,18] Purchased acetonitrile (AN) and ac-

[⊗] Abstract published in *Advance ACS Abstracts,* February 1, 1997.

S0024-9297(96)01123-0 CCC: $14.00

Table 1. Characteristics of the PMMA-*g*-PS Sample[16]

	backbone		branch				
$10^6 M_w$[a]	$10^6 M_w$[b]	M_w/M_n[c]	$10^3 M_w$[c]	M_w/M_n[c]	av PS composition[c] $\langle W \rangle$	m[d]	M_{sc}[e]
6.69	5.58	<1.10	9.19	1.04	0.128	93.2	6.26

[a] Averaged value of apparent molecular weight measured by SLS in 1-ethylnaphtharene, isoamyl acetate, and chloroform. [b] Measured by SLS. [c] Measured by ^{1}H NMR. [d] Average number of branches per molecule calculated from $M_w\langle W \rangle/M_w$(branch). [e] Average molecular weight between nearest-neighbor branch points calculated from $M_w(1 - \langle W \rangle)/m$.

etoacetic acid ethyl ester (AAEE) were dried over calcium hydride and purified by distillation. The mixed solvent has the composition [AN]:[AAEE] = 3:1 (in weight), is a marginally-good solvent to PMMA (the Θ-temperature is a little lower than 10 °C), and is a nonsolvent to PS.[17]

Light Scattering Measurements. The stock solution was prepared by dissolving the graft copolymer in AAEE, adding AN to give the desired solvent composition, mildly stirring at room temperature for 2 h, and keeping the solutions around 60 °C for 1 day. The stock solution was filtered at 60 °C through a Millipore filter (pore size: 3.0 μm) into light scattering cells, followed by dilution with dust-free mixed solvent to make sample solutions with desired concentration c ranging from 1×10^{-4} to 8×10^{-4} g (g of solution)$^{-1}$. Subsequently, the optical cells were flame-sealed under a mild vacuum and were left around 60 °C for 1 day for the sake of equilibrium of the solution before light scattering measurements.

The light scattering apparatus was a specially-designed one with an Ar-ion laser operating at the wavelength of 488 nm as the light source. The correlator used in dynamic light scattering was a Multiple-Tau Digital Correlator, ALV-5000. Details of the light scattering spectrometer have been described elsewhere.[19] Analysis of the light scattering data was made in the same way as in the previous study.[17]

The excess Rayleigh ratio $R_{vv}(\theta)$ was calculated from the measured excess scattered intensity as a function of scattering angle θ. Since, in the time-resolved measurement, the conventional analysis with extrapolation of the concentration to the dilute limit is not available, we have evaluated the apparent molecular weight M_{app} and apparent radius of gyration R_{gapp} without the extrapolation, which are defined as

$$M_{app} = \frac{R_{vv}(0)}{KC} \tag{1}$$

$$R_{gapp}{}^2 = \frac{(\text{initial slope})M_{app}}{q^2/3} \tag{2}$$

where the constant K is given by $K = 4\pi^2 n^2 (\partial n/\partial C)^2/(N_A \lambda_0^4)$, with n being the refractive index of solvent, N_A the Avogadro constant, $(\partial n/\partial C)$ the refractive index increment, and λ_0 the wavelength of the incident beam in vacuum, and the momentum transfer q is given by $q = (4\pi n/\lambda_0) \sin(\theta/2)$. The concentration C is in weight per volume of solution. $KC/R_{vv}(0)$ and (initial slope) are the intercept and the initial slope of $KC/R_{vv}(\theta)$ vs q^2 plots at *finite* concentration. The value of R_{gapp} is the refractive-index-increment-weighted one in the copolymers. In the present case, however, the scattered light intensity of the PMMA backbone dominates over that of PS branches because of the low branch composition, so that the obtained R_{gapp} can practically be regarded as a true radius of gyration of the z-average. The apparent particle scattering factor $P_{app}(q)$ has also been calculated by

$$P_{app}(q) = R_{vv}(q)/R_{vv}(0) \tag{3}$$

The correlation function of the electric field obtained from the autocorrelation function of scattered light intensity approximately followed a single exponential decay and allowed us to obtain the decay rate Γ by the second-order cumulant method.[20] The diffusion coefficient D was calculated by $D = \Gamma/q^2$ and then was extrapolated to $q = 0$, if D depended on q; otherwise, D at 30° was regarded as those at $q = 0$. The obtained D was transformed to the hydrodynamic radius R_h by the Einstein−Stokes equation

$$R_h = \frac{kT}{6\pi\eta D} \tag{4}$$

where k, T, and η are the Boltzmann constant, absolute temperature, and solvent viscosity, respectively. Similarly to the static properties, we evaluated the hydrodynamic radius without the extrapolation, which was here referred to as the apparent hydrodynamic radius R_{happ}.

Results and Discussion

Intermolecular Association. Figure 2 shows the temperature dependence of M_{app}, R_{gapp}, and R_{happ} for the copolymer solutions of various concentrations under cooling at the rate of 2.5 or 10 °C/h. It has been demonstrated in the previous study that, in the solution of the lowest copolymer concentration [1.38×10^{-4} g (g of solution)$^{-1}$], unimolecular micelles of a rigid-rod-like string of a few linearly-connected flowers (see Figure 1b) are formed with decreasing temperature.[17] At the copolymer concentration $c = 2.74 \times 10^{-4}$ g (g of solution)$^{-1}$, M_{app}, R_{gapp}, and R_{happ} have almost the same magnitude as those at the lowest copolymer concentration, suggesting that a unimolecular micelle is formed with decreasing temperature. On the other hand, at higher concentrations, M_{app} increases with decreasing temperature to be larger than that of the unimer at lower temperatures, which clearly shows that intermolecular associates are formed. The association number is around 3 at 10 °C. With decreasing temperature, R_{gapp} decreases gradually, while R_{happ} increases. These temperature dependences of R_{gapp} and R_{happ} differ from those at the lower copolymer concentrations which may imply that the shrinkage of the associating polymer chains and the segregation between PS and PMMA chains in an associate are accompanied by an increase of the association number and lead to the multimolecular-micelle formation as the temperature decreases.

Figure 3 shows the time dependence of M_{app}, R_{gapp}, and R_{happ} in log−log scale for the copolymer solutions of various concentrations after quenching from 60 to 30 °C. M_{app}, R_{gapp}, and R_{happ} show no change with time for 10 days for all concentrations, having almost the same values, respectively, as those observed at 30 °C in the cooling process (see Figure 2). This result suggests that what we have observed are structures at quasi-equilibrium or the equilibrium state. On the other hand, continuation of the intermolecular association is observed at lower temperatures. Figure 4 shows the results for the copolymer solution of $c = 7.92 \times 10^{-4}$ g (g of solution)$^{-1}$ after quenching from 60 to 21 °C. The multimolecular micellization progresses and does not reach an equilibrium within the experimental time scale. The association number of the micelle changes from 2 to 11 with the lapse of time. Parts a and b of Figure 5 show plots of R_{gapp} and R_{happ} against M_{app} for these data along with those at 20 °C in the cooling process (see Figure 2). R_{gapp} and R_{happ} monotonously increase with increasing M_{app}, and all points of the data

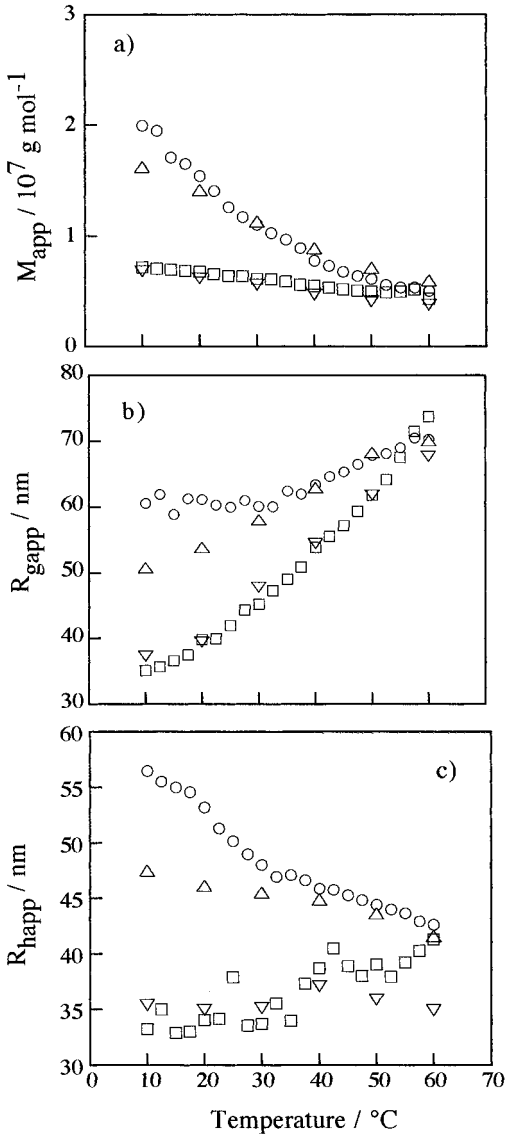

Figure 2. Change of M_{app} (a), R_{gapp} (b), and R_{happ} (c) with decreasing temperature for the copolymer solutions of various concentrations: (○) 7.92×10^{-4} g (g of solution)$^{-1}$; (△) 5.03×10^{-4} g (g of solution)$^{-1}$; (▽) 2.74×10^{-4} g (g of solution)$^{-1}$; (□) 1.38×10^{-4} g (g of solution)$^{-1}$.

fall approximately on respective single master curves. These parallel changes of R_{gapp} and R_{happ} with change of M_{app} suggest that the association proceeds with growth of the association-micelle size with almost no change of micellar fraction.[21] In other words, most of copolymers form micelles with similar size and there remains no appreciable amount of unimers in solution. This is also supported by the fact that no particular increase of the particle-size-distribution index μ_2/Γ^2 is detected with increasing M_{app}. Therefore it is considered that apparent quantities M_{app}, R_{gapp}, and R_{happ} approximately represent those of micelles themselves. Discussion hereafter will be made on this basis.

***M*$_{app}$ Dependence of *R*$_{gapp}$, *R*$_{happ}$, and *R*$_{gapp}$/*R*$_{happ}$ of Multimolecular Micelles.** The master curve in Figure 5a or b is described by a power law $R_{gapp} \propto M_{app}{}^{\nu_g}$ with $\nu_g = 0.717$ or $R_{h,app} \propto M_{app}{}^{\nu_h}$ with $\nu_h = 0.414$. The difference between ν_g and ν_h leads to the characteristic M_{app} dependence of the ratio R_{gapp}/R_{happ}, as shown in Figure 5c, where R_{gapp}/R_{happ} values are plotted against M_{app} in semilog plots. The ratio rapidly increases with increasing M_{app}. Large values (>2) of the ratio at higher molecular weights suggest a rod-like structure of the

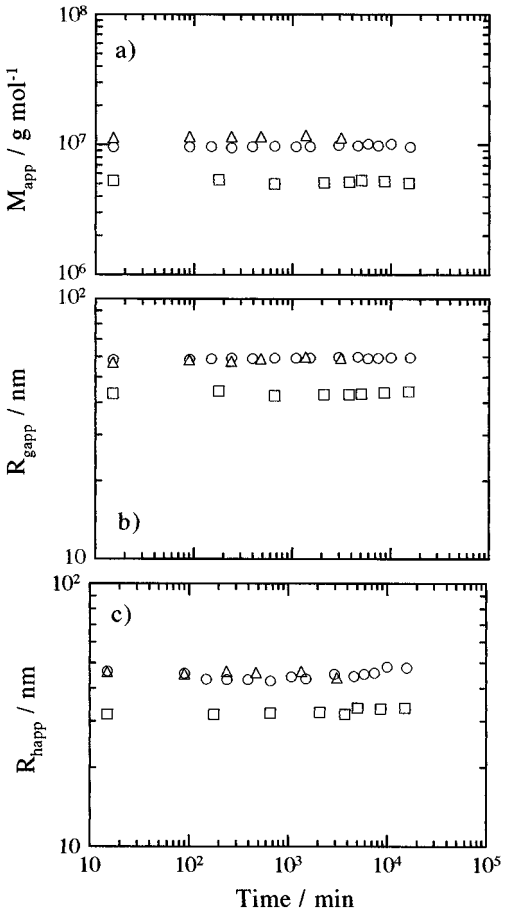

Figure 3. Time evolution of M_{app} (a), R_{gapp} (b), and R_{happ} (c) after quenching the copolymer solutions of various concentrations from 60 to 30 °C: (○) 7.92×10^{-4} g (g of solution)$^{-1}$; (△) 5.03×10^{-4} g (g of solution)$^{-1}$; (□) 1.38×10^{-4} g (g of solution)$^{-1}$.

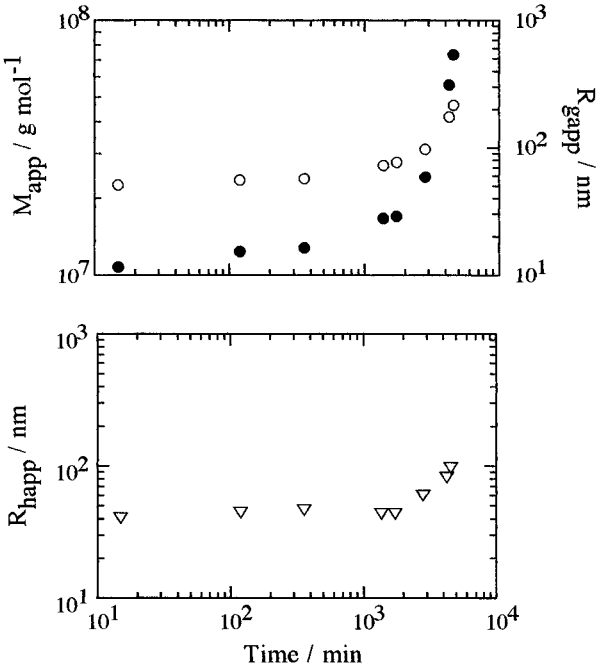

Figure 4. Time evolution of M_{app} (●), R_{gapp} (○), and R_{happ} (▽) after quenching the copolymer solution of $c = 7.92 \times 10^{-4}$ g (g of solution)$^{-1}$ from 60 to 21 °C.

large contour length and the large persistence length.[22] Seeing the results in Figure 5c more closely, one can notice that the ratio is almost independent of M_{app} in the low molecular weight region (6×10^6 to 1.5×10^7).

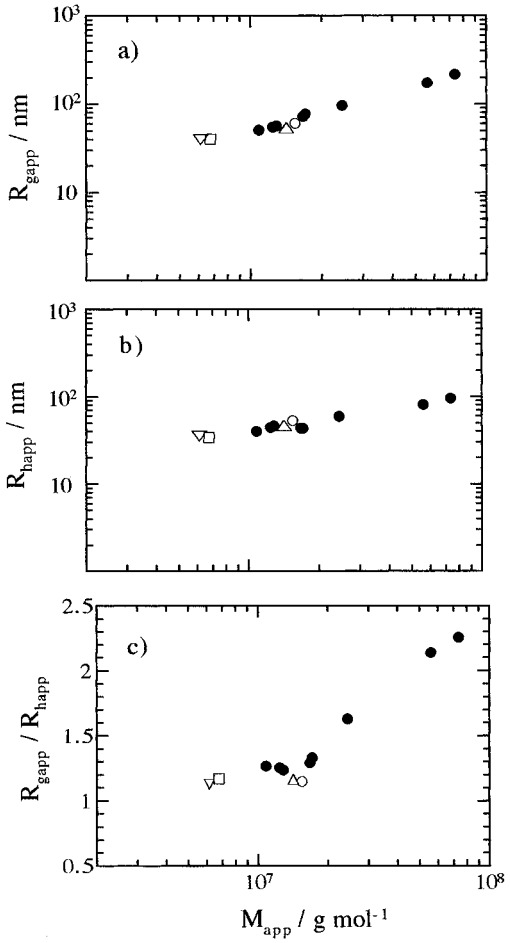

Figure 5. M_{app} dependence of R_{gapp} (a), R_{happ} (b), and R_{gapp}/R_{happ} (c) for the data of time dependence after quenching the copolymer solution of $c = 7.92 \times 10^{-4}$ g (g of solution)$^{-1}$ from 60 to 21 °C (●): (○) 7.92×10^{-4} g (g of solution)$^{-1}$; (△) 5.03×10^{-4} g (g of solution)$^{-1}$; (▽) 2.74×10^{-4} g (g of solution)$^{-1}$; (□) 1.38×10^{-4} g (g of solution)$^{-1}$. Open symbols are measured values at 20 °C under the cooling process.

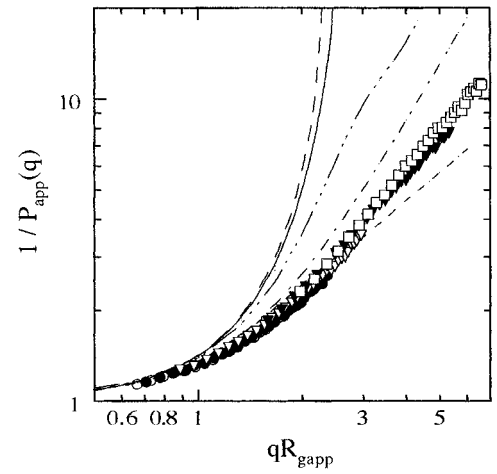

Figure 6. Scattering vector q dependence of the apparent scattering function P_{app} of the multimolecular micelles formed at 21 °C in the form of $1/P_{app}(q)$ vs $R_{gapp}q$ plot: (○) 1380 min; (●) 1740 min; (▽) 2820 min; (▼) 4260 min; (□) 4590 min. The curves are calculated using a uniform sphere(—), a hollow sphere with an infinitely-thin shell (— —), the Gaussian chain (— · —), an infinitely-thin disk (— ···), and a rigid rod with an infinitely-small thickness (- - -).

Apparent Particle-Scattering Factors of Multimolecular Micelles. Figure 6 shows a comparison of apparent particle-scattering factors $P_{app}(q)$ of the multimolecular micelles formed at 21 °C with calculated ones of some selected model structures[23,24] in plots of $1/P_{app}(q)$ as a function of qR_{gapp}. The model structures are uniform sphere, hollow sphere with an infinitely-thin shell, the Gaussian chain (the Debye function), infinitely-thin disk, and rigid rod with infinitely-small thickness. The $P_{app}{}^{-1}$ of the micelles are reproduced most closely by the calculated particle-scattering factor of the rigid rod. At large qR_{gapp}, $1/P_{app}(q)$ values at time = 4260 and 4590 min deviate upward from the calculated one. The deviation may come from a finite thickness and a finite persistence length of the micelle. By taking the thickness and/or the flexibility into account, the calculated particle-scattering factor of the rigid rod structure becomes larger at large qR_{gapp}, so that the deviation becomes smaller.

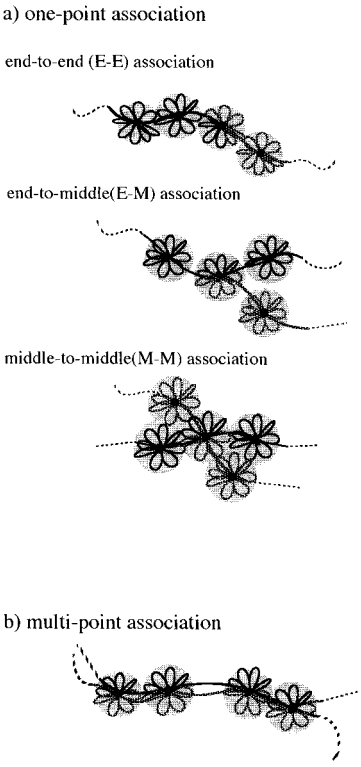

Figure 7. Schematic illustration of possible ways of intermolecular association between unimolecular micelles of graft copolymer. See text for details.

Possible Ways of Association and the Most Plausible Structure of the Associate. Once the multimolecular micelle is formed in this system, the unimolecular micelle can adopt two different ways of intermolecular association, that is, one-point association and multipoint association, which are illustrated in Figure 7. The one-point association is divided into three types depending upon where the intermolecular association takes place, i.e., association between end points [end-to-end (E−E) association], between end point and middle point [end-to-middle (E−M) association], and between middle points [middle-to-middle (M−M) association]. Each form of intermolecular association leads to a different structure of the multimolecular micelle, as shown in Figure 8. Micellization by E−E association or the multipoint association (Figure 7b) leads to formation of a multimolecular micelle made of linearly-connected flowers (a, f), while a star-shaped associate (b) can be formed by M−M association. E−M association produces linear (d) and/or branched (c) associates. If many E−M associations take place in one

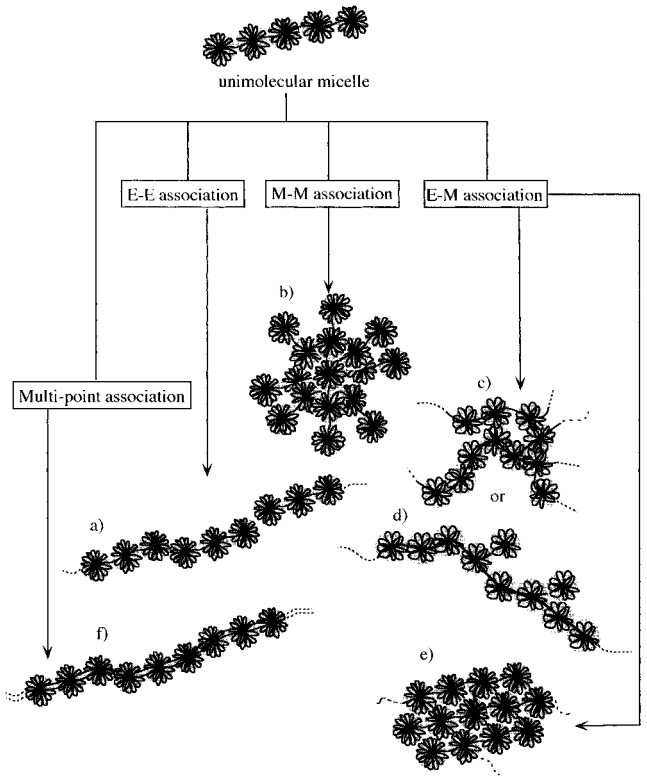

Figure 8. Schematic illustration of structures of multimolecular micelles formed by E−E association, E−M association, M−M association, and multipoint association. Micellization by E−E association and multipoint association leads to the formation of a multimolecular micelle made of linearly-connected flowers (a, f), while a star-shaped associate can be formed by M−M association (b). E−M association produces a linear and/or branched associate (c, d). A collapsed network chain of flowers (e) can be formed by the occurrence of many E−M associations in one associate.

associate, a compact globule (e) consisting of collapsed network chains of flowers[25] is possibly formed.

Notable experimental results are the large values of ν_g (=0.717) and R_{gapp}/R_{happ} compared with those of the dense structures,[26,27] and the particle-scattering function $P_{app}(q)$ is similar to that of rigid rod (see Figures 5 and 6). These facts exclude the formation of compact globule, star-shaped, and branched associates but suggest the micellar structure to be a rod-like associate with a large persistence length. Therefore, structures a, f, and d in Figure 8, which are formed by E−E, multipoint, and E−M associations, respectively, remain as the possible structure.

For the multimolecular micelles formed by the multipoint association, the number P (=NP_u) of flowers per micelle is related to the number n_p of petals per flower and the number m of branches per molecule as $P = Nm/(n_p + N)$, where N and P_u are the association number and the number of flowers per molecule, respectively. On the other hand, the relation $P = Nm/(n_p + 1)$ holds for those formed by E−E association. If N is relatively small at fixed n_p, the difference of P between these micelles is so small, since $N \ll n_p$, that the dimensions of the micelles should have almost the same magnitude, and we cannot distinguish these two types of micelles. However, multipoint association may bring about loss of the conformational entropy so that the micelle formed by E−E association is more stable. Thus, structure f may also be rejected.

In the following section, we will analyze the experimental data using the rigid-rod model and worm-like chain model to reveal more detail on the form of association and the structure of the associates.

Quantitative Analyses by the Rigid-Rod Model and Worm-like Chain Model. The radius $R_{g,RR}$ of gyration and hydrodynamic radius $R_{h,RR}$ of a uniform rigid rod with hemispheres at its ends are given as a function of the contour length L_e and the radius of the cross section R_{cs} by[17,28]

$$R_{g,RR}^2 = \frac{\frac{4}{5}R_{cs}^5 + (L_e - 2R_{cs})R_{cs}^4 + \frac{1}{3}(L_e - 2R_{cs})2R_{cs}^3 + \frac{1}{12}(L_e - 2R_{cs})^3R_{cs}^2}{(L_e - 2R_{cs})R_{cs}^2 + \frac{4}{3}R_{cs}^3} \quad (5)$$

$$\frac{L_e}{2R_{h,RR}} = \ln\frac{2L_e - 2R_{cs} + \{4L_e^2 - 4L_e(2R_{cs}) + 2(2R_{cs})^2\}^{1/2}}{2R_{cs}} + \frac{L_e + 2^{1/2}(2R_{cs}) - \{4L_e^2 - 4L_e(2R_{cs}) + 2(2R_{cs})^2\}^{1/2}}{L_e} + \{(2R_{cs})/2L_e\}\ln\frac{(2^{1/2} - 1)^2[2R_{cs} + \{4L_e^2 - 4L_e(2R_{cs}) + 2(2R_{cs})^2\}^{1/2}]}{2L_e - 2R_{cs} + \{4L_e^2 - 4L(2R_{cs}) + 2(2R_{cs})^2\}^{1/2}} \quad (6)$$

In the case of structure a in Figure 8, R_{cs} corresponds to the radius of a flower and L_e is expressed as $L_e = 2R_{cs}P_uN$ with the total number P_uN of flowers in one micelle. Using eqs 5 and 6, we can calculate the molecular-weight (or association number) dependence of the radius of gyration and hydrodynamic radius of the multimolecular micelle for a given number of P_u, if R_{cs} is estimated for the given P_u. The molecular weight M of the micelle is calculated from $M = M_uN$, where M_u is the molecular weight of the graft copolymer. The radius of gyration of a flower is assumed to be equal to $R_{g,star}$ of the star-shaped polymer made of arms of molecular weight $M_{sc}/2$ with the arm number $f = 2m/P_u$, where M_{sc} is the molecular weight of PMMA subchains between the nearest-neighbor branch points (see Table 1). Namely, R_{cs} is assumed to be given by $R_{cs}^2 = (5/3)R_{g,star}^2$. $R_{g,star}$ can be estimated from the fact that the ratio $g_{ga} = R_{g,star}/R_{g,arm}$ depends on the arm number f only, where $R_{g,arm}$ is the radius of gyration of the arm polymer as it is a free chain.[26,29−33] Noticing that solvent quality to PMMA is near the Θ-condition,[17] we use the $R_{g,star}$ value and g_{ga} expression at the Θ-condition. The radius $R_{g,arm}$ is calculated to be 4.71 nm,[17] and the value of g_{ga} is evaluated with the experimental equation $g_{ga} = (1.27)^{0.5}f^{0.220}$ for $4 < f < 269$.[33]

In Figure 9, M_{app} (or N_{app}) dependences of R_{gapp}, R_{happ} and R_{gapp}/R_{happ} are compared with calculated ones with $P_u = 4-6$, where the apparent association number N_{app} is given by M_{app}/M_u. R_{gapp}, R_{happ}, and R_{gapp}/R_{happ} of unimolecular micelles ($N_{app} = 1$) are almost reproduced by the calculated ones with $P_u = 5$. The number $P_u = 5$ is larger than $P_u = 3.7$ estimated for the unimolecular micelle formed at 10 °C in the previous study.[17] This is reasonable because the present micelles were formed at the higher temperature 21 °C. The larger value of P_u (or smaller n_p) may come from the increase of excluded volume of the backbone chain and the decrease of attractive interaction between the branch PS segments with increasing temperature. With increasing molecular weight, both $R_{g,RR}$ and $R_{h,RR}$ monotonously increase and the ratio $R_{g,RR}/R_{h,RR}$ rapidly increases to the value of more than 2, which are consistent with the experimental results. However, in the region of $N_{app} >$ 2, the experimental values of any quantities are smaller

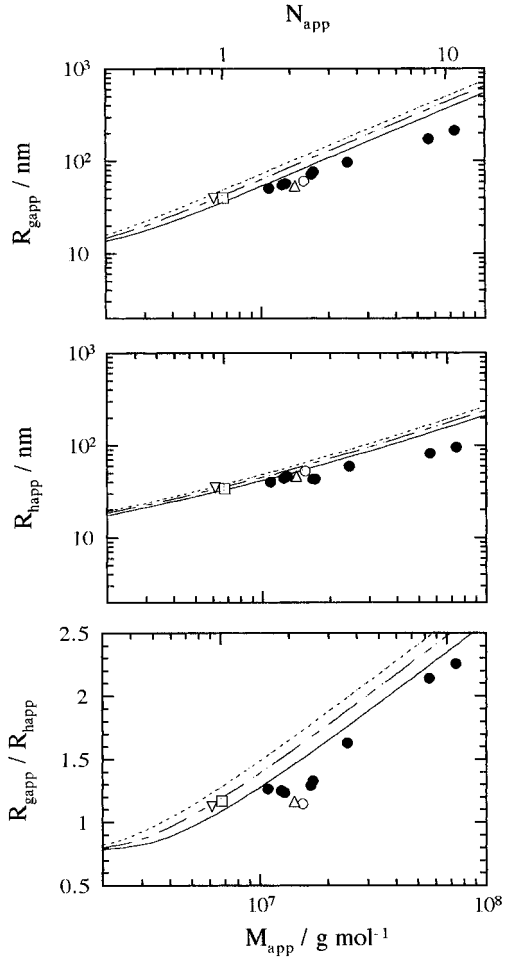

Figure 9. Applicability of the rigid-rod model to the light scattering data shown in Figure 5. The number P_u of flowers per molecule is $P_u = 4$ (—), 5 (—·—), or 6 (···).

than the calculated ones. More quantitatively, the experimental values of $N_{app} > 2$ are almost superposed on the calculated curves by shifting R_{gapp}, R_{happ}, and R_{gapp}/R_{happ} to a higher association number by the factor of $N_{app} \sim 2$.

The form of association and the structure of the associates expected from the above comparisons are schematically illustrated in Figure 10. Intermolecular association proceeds by successive occurrences of E−M and E−E associations. E−M association may take place in the first association ($N_{app} \sim 2$) or after two or more successive E−E associations to form branched associates, but two or more successive E−M may not take place easily due to the excluded-volume effect. As a consequence, these two association types take place almost alternately, and the associates of higher association numbers have short branches but are of long rod-like structure as a whole. The presence of short branches by E−M association is responsible for the shift of R_{gapp}/R_{happ}, R_{gapp}, and R_{happ} to the higher association number. A little weaker M_{app} dependences of R_{gapp} and R_{happ} may be owing to the flexibility of the associates because such long rod-like micelles may be somewhat flexible.

To evaluate the flexibility, a worm-like chain model is here adopted as a rod-like particle with a finite persistence length. The radius $R_{g,WC}$ of gyration of an infinitely-thin worm-like chain is given as a function of the contour length L_e and the persistence length λ by Porte et al. as follows.[34]

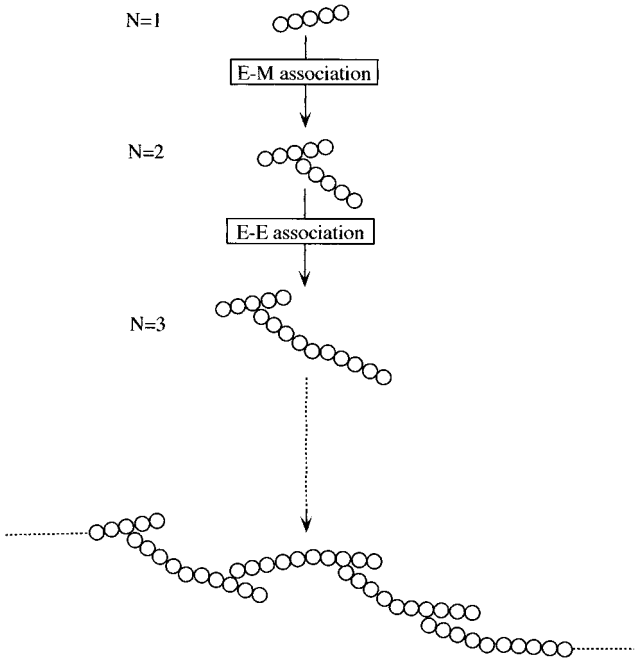

Figure 10. Schematic illustration of the supposed association of rigid-rod-like unimolecular micelles which are made of linearly-connected flowers. E−M association takes place until $N \sim 2$ to form a branched associate, but the next molecule connects to the associate by E−E association, and these two forms of association continue almost alternately.

$$R_{g,WC}^2 = \lambda^2\left[(L_e/3\lambda) - 1 + 2(\lambda/L_e) - 2\left(\frac{1 - \exp(-L_e/\lambda)}{(L_e/\lambda)^2}\right)\right] \quad (7)$$

Effects of finite thickness on the radius of gyration is neglected here, and eq 7 is used with no correction for the thickness. The estimated discrepancy of eq 7 from eq 5 is less than 5% for the rigid-rod-like unimolecular micelle with $P_u = 5$, and the discrepancy decreases with increasing contour length. The hydrodynamic radius $R_{h,WC}$ of a worm-like chain with hemispheres at its ends is given as a function of L_e, R_{cs}, and λ as follows, according to the calculation by Norisuye et al.[28]

$$R_{h,WC} = \frac{L_e}{2}\{C_1 \ln(L_e/2R_{cs}) + C_2 + C_3(L_e/2\lambda) + C_4(L_e/2\lambda)^2 + C_5(L_e/2\lambda)^3 + C_6(L_e/2\lambda)^4 + C_7(L_e/2\lambda)^5 + ...\}^{-1} \quad (8)$$

Here, C_i ($i = 1-7$) are given as a function of $2R_{cs}/L_e$. Equation 7 is available for the condition of $L_e/2\lambda < 2.278$. In the case of $L_e/2\lambda > 2.278$, we use Yamakawa's equation for hydrodynamic radius $R_{h,WC}$ of a worm-like chain with no hemisphere at its ends,[35] which is expressed as

$$R_{h,WC} = \frac{L_e}{2}\{A_1(L_e/2\lambda)^{1/2} + A_2 + A_3(L_e/2\lambda)^{-1/2} + A_4(L_e/2\lambda)^{-1} + A_5(L_e/2\lambda)^{-3/2} + ...\}^{-1} \quad (9)$$

where A_i ($i = 1-5$) are given as functions of $2R_{cs}/L_e$. In the calculation of $R_{h,WC}$, eq 8 is used for $L_e \gg R_{cs}$, where the effect of hemispheres on $R_{h,WC}$ can reasonably be neglected. In Figure 11, the experimental results are compared with calculated ones with $\lambda = 500$ and 100 nm at $P_u = 5$. Those for rigid-rod structure calculated

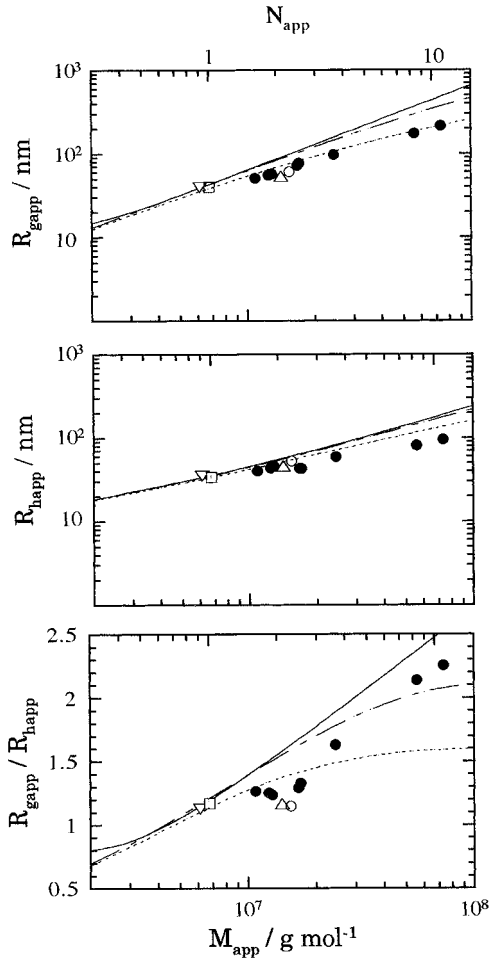

Figure 11. Applicability of the worm-like chain model to the light scattering data shown in Figure 5: (—·—) $\lambda = 500$ nm, $P_u = 5$; (····) $\lambda = 100$ nm, $P_u = 5$; (—) calculated curve using the rigid-rod model with $P_u = 5$.

from eqs 5 and 6 with $P_u = 5$ are also shown in the same figure. M dependences of $R_{g,RR}$, $R_{h,RR}$, and $R_{g,RR}/R_{h,RR}$ become weaker with decreasing persistence length. Taking the shift of the N_{app} scale due to the short branches into consideration, discrepancy between the experimental values and calculated curves is largest at $\lambda = 100$ nm. Even at $\lambda = 500$ nm, $R_{g,RR}/R_{h,RR}$ gets to the top around $M = 10^8$, which is inconsistent with the experiments. Therefore, the persistence length of the multimolecular micelle may be more than several hundreds of nanometers. The rigid-rod model produces the value of $R_{g,WC}/R_{h,WC} = 2$ at $L_e/2R_{cs} = 730$ nm/30.4 nm = 24, and the value of 2 is also reproduced by the worm-like chain model of $\lambda = 500$ nm at $L_e/2R_{cs} = 1216$ nm/30.4 nm = 40 and $L_e/\lambda = 1216$ nm/500 nm = 2.4. Thus, the multimolecular micelles of $N_{app} \sim 10$ are expected to have a large axis ratio and a high rigidity. More quantitatively, the shape and size of the micelle as a whole must be expressed by effective parameters of the radius of cross section $R_{cs,eff}$, the contour length $L_{e,eff}$, and the persistence length λ_{eff}, because the micelles must have short branches. Comparing with R_{cs}, L_e, and λ of the rod-like associate with no branch formed by E−E association only, $R_{cs,eff}$ and λ_{eff} are larger, while $L_{e,eff}$ is smaller. Therefore, the ratios $L_{e,eff}/2R_{cs,eff}$ and $L_{e,eff}/\lambda_{eff}$ of the associates of $N_{app} \sim 10$ may be smaller than those of the models calculated above.

References and Notes

(1) Tuzar, Z.; Kratochivil, P. In *Surface and Colloid Science*; Matijevic, E., Ed.; Plenum Press: New York, 1993; Vol. 15, p 1.
(2) Leibler, L.; Oriand, H.; Wheeler, J. C. *J. Chem. Phys.* **1983**, *79*, 3550.
(3) ten Brinke, G.; Hadziioannou, G. *Macromolecules* **1987**, *20*, 1986.
(4) Honda, C.; Sakaki, K.; Nose, T. *Polymer* **1994**, *35*, 5309.
(5) Balsara, N. P.; Tirrell, M.; Lodge, T. P. *Macromolecules* **1991**, *24*, 1975.
(6) Zhou, Z.; Chu, B.; Peiffer, D. G. *Macromolecules* **1993**, *26*, 1876.
(7) Schillen, K.; Brown, W.; Konak, C. *Macromolecules* **1993**, *26*, 3611.
(8) Raspand, E.; Lairez, D.; Carton, J.-P. *Macromolcules* **1994**, *27*, 2956.
(9) Dondos, A.; Remp, P.; Benoit, H. *J. Chim. Phys.* **1965**, *62*, 821.
(10) Dondos, A.; Remp, P.; Benoit, H. *J. Polym. Sci., Polym. Lett. Ed.* **1966**, *4*, 293.
(11) Selb, J.; Gallot, Y. In *Plymeric Amines and Ammonium Salts*; Goethals, E. J., Ed.; Pergamon Press: Oxford, U.K., 1980.
(12) Price, C.; Woods, D. *Polymer* **1973**, *14*, 82.
(13) Price, C.; Woods, D. *Polymer* **1974**, *15*, 389.
(14) Gallot, T.; Franta, E.; Remp, P.; Benoit, H. *J. Polym. Sci. Part C* **1964**, *4*, 473.
(15) Bresler, S. E.; Pyrkov, L. M.; Frenkel, S. Ya.; Laius, L. A.; Klenin, S. I. *Vysokomol. Soedin.* **1962**, *4*, 250.
(16) Kikuchi, A.; Nose, T. *Polymer*, in press.
(17) Kikuchi, A.; Nose, T. *Macromolecules* **1996**, *29*, 6770.
(18) Kikuchi, A.; Nose, T. *Polymer* **1995**, *36*, 2781.
(19) Varma, B.; Fujita, Y.; Takahashi, M.; Nose, T. *J. Polym. Sci., Polym. Phys. Ed.* **1984**, *22*, 1181.
(20) Koppel, D. E. *J. Chem. Phys.* **1974**, *57*, 4814.
(21) Honda, C.; Hasegawa, Y.; Hirunuma, R.; Nose, T. *Macromolecules* **1994**, *27*, 7660.
(22) Kubota, K.; Tominaga, Y.; Fujime, S. *Macromolecules* **1986**, *19*, 1604.
(23) Benoit, H.; Frolich, D. In *Light Scattering from Polymer Solutions*; Huglin, M. B., Ed.; Academic Press: London, 1972; Chapter 11.
(24) Burchard, W. *Adv. Polym. Sci.* **1983**, *48*, 53.
(25) Semenov, A. N.; Joanny, J.-F.; Khokhlov, A. R. *Macromolecules* **1995**, *28*, 1066.
(26) Takano, A.; Okada, M.; Nose, T. *Polymer* **1992**, *33*, 783.
(27) Daoud, M.; Joanny, F. *J. Physique* **1981**, *42*, 1359.
(28) Norisuye, T.; Motowoka, M.; Fujita, H. *Macromolecules* **1979**, *12*, 320.
(29) Zimm, B. H.; Stockmayer, W. H. *J. Chem. Phys.* **1949**, *17*, 1301.
(30) Miyake, A.; Freed, K. F. *Macromolecules* **1983**, *16*, 1228.
(31) Douglas, J. F.; Freed, K. F. *Macromolecules* **1984**, *17*, 2344.
(32) Douglas, J. F.; Roovers, J.; Freed, K. F. *Macromolecules* **1990**, *23*, 4168.
(33) Roovers, J. E. L.; Toporowski, P.; Martin, J. *Macromolecules* **1989**, *22*, 1897.
(34) Porte, G.; Appell, J.; Poggl, Y. *J. Phys. Chem.* **1980**, *84*, 3105.
(35) Yamakawa, H.; Fujii, M. *Macromolecules* **1973**, *6*, 407.

MA9611230